

Cite this: *Chem. Sci.*, 2022, 13, 13764

All publication charges for this article have been paid for by the Royal Society of Chemistry

Room temperature chemoselective hydrogenation of C=C, C=O and C=N bonds by using a well-defined mixed donor Mn(I) pincer catalyst†

Anand B. Shabade,^{ab} Dipesh M. Sharma,^{ab} Priyam Bajpai,^{bc}
Rajesh G. Gonnade,^{bd} Kumar Vanka^{bc} and Benudhar Punji^{ab}*

Chemoselective hydrogenation of C=C, C=O and C=N bonds in α,β -unsaturated ketones, aldehydes and imines is accomplished at room temperature (27 °C) using a well-defined Mn(I) catalyst and 5.0 bar H₂. Amongst the three mixed-donor Mn(I) complexes developed, $\kappa^3\text{-(R}^2\text{PN}^3\text{N}^{\text{Pyz}}\text{)Mn(CO)}_2\text{Br}$ (R = Ph, ⁱPr, ^tBu); the ^tBu-substituted complex (^tBu₂PN³N^{Pyz})Mn(CO)₂Br shows exceptional chemoselective catalytic reduction of unsaturated bonds. This hydrogenation protocol tolerates a range of highly susceptible functionalities, such as halides (–F, –Cl, –Br, and –I), alkoxy and hydroxy, including hydrogen-sensitive moieties like acetyl, nitrile, nitro, epoxide, and unconjugated alkenyl and alkynyl groups. Additionally, the disclosed method applies to indole, pyrrole, furan, thiophene, and pyridine-containing unsaturated ketones leading to the corresponding saturated ketones. The C=C bond is chemoselectively hydrogenated in α,β -unsaturated ketones, while the aldehyde's C=O bond and imine's C=N bond are preferentially reduced over the C=C bond. A detailed mechanistic study highlighted the non-innocent behavior of the ligand in the (^tBu₂PN³N^{Pyz})Mn(I) complex and indicated a metal–ligand cooperative catalytic pathway. The molecular hydrogen (H₂) acts as a hydride source, whereas MeOH provides a proton for hydrogenation. DFT energy calculations supported the facile progress of most catalytic steps, involving a crucial turnover-limiting H₂ activation.

Received 21st September 2022
Accepted 2nd November 2022

DOI: 10.1039/d2sc05274a

rsc.li/chemical-science

Introduction

Chemoselective hydrogenation of unsaturated organic compounds is extremely important in academia and industry, as it plays a crucial role in the preparation of pharmaceutical intermediates, fragrances, fine chemicals and various bulk products. Particularly, the catalytic reductions using molecular hydrogen under ambient conditions represent one of the economical, atom-efficient and environmentally benign transformations.¹ In this context, numerous heterogeneous catalysts are developed and demonstrated for the hydrogenation of various functional groups, which often require high reaction temperatures and/or pressures and result in poor selectivity.² Over time, many well-defined, active and highly efficient

homogeneous catalysts,³ derived from precious and non-precious transition metals, have been established for hydrogenation.⁴ In general, noble metal catalysis has dominated the field and accomplished very high catalytic turnovers and desired selectivity. However, the limited availability of noble metals in the earth's crust, and their expensiveness and underlying toxicity could limit their wide applications in hydrogenation in the future.

One of the fundamental research objectives in modern science is environmental benignity and sustainable development. Accordingly, the hydrogenations by catalysts based on low-toxic, earth-abundant and inexpensive non-precious metals have been given significant consideration.⁵ Particularly, the hydrogenations employing iron,⁶ cobalt⁷ and nickel^{6c} are substantially explored and disclosed as active and highly efficient for reducing carbonyls, imines and nitriles.⁸ Being a less toxic, cheap and the third most abundant transition metal, manganese is elegantly demonstrated as a catalyst for the hydrogenation of aldehydes/ketones by Beller,⁹ Kempe,¹⁰ Sortais,¹¹ Kirchner¹² and others (Scheme 1a).^{13,14} Similarly, the hydrogenation of imines (or C=N bond) using bidentate or pincer-ligated manganese catalysts was established.¹⁵ Meanwhile, the independent development of chiral pincer-manganese catalysts by Clarke,¹⁶ Beller,¹⁷ Han/Ding¹⁸ and others¹⁹ led to the asymmetric hydrogenation of ketones. In

^aOrganic Chemistry Division, CSIR-National Chemical Laboratory (CSIR-NCL), Dr Homi Bhabha Road, Pune 411008, India. E-mail: b.punji@ncl.res.in

^bAcademy of Scientific and Innovative Research (AcSIR), Ghaziabad 201002, India

^cPhysical and Material Chemistry Division, CSIR-NCL, Dr Homi Bhabha Road, Pune, India

^dCentre for Material Characterization, CSIR-NCL, Dr Homi Bhabha Road, Pune, India

† Electronic supplementary information (ESI) available: Full experimental procedures and characterization data, including ¹H and ¹³C NMR of all compounds, CIF and DFT (.xyz) file]. CCDC 2194541 (for comp. Mn-2). For ESI and crystallographic data in CIF or other electronic format see DOI: <https://doi.org/10.1039/d2sc05274a>





Scheme 1 Manganese-catalyzed hydrogenation of unsaturated bonds: (a) carbonyls and imines, (b) C=C bond, and (c) chemoselective hydrogenation of C=C, C=O, and C=N bonds.

a significant advancement, Liu has shown the asymmetric hydrogenation of the C=N bond in heteroaromatics using a chiral Mn-catalyst.²⁰ Despite all developments on the Mn-catalyzed hydrogenations of multiple polar bonds, the chemoselective hydrogenation of C=C bonds is highly challenging and extremely rare due to the associated high bond enthalpies. The group of Kirchner and Khusnutdinova independently used bidentate PP- and PN-ligated Mn(I) catalysts for the hydrogenation of alkenes using 50 bar and 30 bar H₂ pressures, respectively, at elevated temperatures (Scheme 1b).²¹ Similarly, Topf has demonstrated C=C hydrogenation in α,β -unsaturated carboxylic derivatives using 30–50 bar H₂ at 100–120 °C; however, this protocol failed to provide chemoselective hydrogenation in α,β -unsaturated ketones.^{13c} Though manganese-based catalysts promoted the hydrogenations of many C=O and C=N bonds and certain C=C bonds,^{11b,13c,21} most of the reactions proceed at a high H₂ pressure and at elevated temperatures, which is a significant drawback for practical applications. Additionally, most Mn-catalyzed hydrogenations require a large amount of a strong base (KO^tBu) as an additive. As yet, a chemoselective hydrogenation protocol for reducing one unsaturated functional moiety in the presence of the other using a beneficial Mn-catalyst at ambient H₂ pressure and temperature is unknown.²²

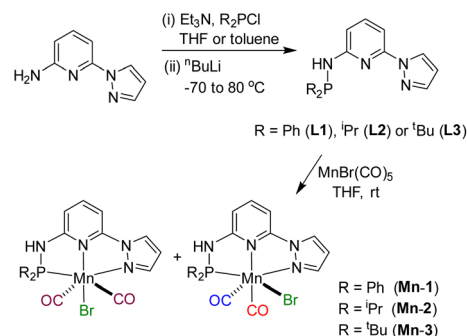
To achieve more sustainability, efficiency and selectivity in Mn-catalysis, in this work, we developed the mixed-donor (PN³N)Mn(I) complexes and disclosed the chemoselective hydrogenation of C=C, C=O and C=N bonds using 5 bar H₂ and a mild base K₃PO₄ at room temperature (Scheme 1c). The notable features of the present protocol are (i) use of the 3rd most abundant transition metal as a catalyst, (ii) excellent

chemoselectivity in the reduction of C=C, C=O and C=N bonds, (iii) hydrogenation using 5 bar H₂ and at room temperature (27 °C), (iv) use of a mild base and atom-efficient H₂ source, and (v) broad substrates scope with excellent tolerance of hydrogen-sensitive functionalities.

Results and discussion

Synthesis of Mn(I) complexes

Based on our expertise in developing pincer-ligated complexes, we became interested in synthesizing mixed-donor PN³N ligands and pincer manganese complexes. We envisioned that a mixed-donor ligand with different electronic features of the donating center could suitably administer the electronic requirement at the metal center and can stabilize the active catalytic species. Moreover, the presence of NH on the side-arm could facilitate the non-innocent behavior of the ligand *via* an aromatization/dearomatization approach leading to the heterolytic activation of molecules. With this in mind, the isopropyl-tagged PN³N ligand **L2** was synthesized in a few steps starting from 2,6-dibromopyridine, following a protocol similar to that for the synthesis of phenyl or *tert*-butyl PN³N ligands **L1** and **L3**.²³ Treatment of pincer ligands **L1**–**L3** with Mn(CO)₅Br in THF at room temperature afforded dicarbonyl Mn(I) complexes, (R²PN³N^{Py}₂)Mn(CO)₂Br; **Mn-1** (R = Ph), **Mn-2** (R = ⁱPr) and **Mn-3** (R = ^tBu), respectively, in good yields (Scheme 2). These complexes were extensively characterized by multinuclear NMR spectroscopy, FT-IR, ESI-MS and elemental analysis. The ³¹P {¹H}-NMR spectra of complexes **Mn-1**, **Mn-2** and **Mn-3** show peaks at 134.5, 136.9; 158.4, 159.8 and 175.3, 178.5 ppm, respectively. Two peaks for each complex at very similar chemical shift values indicate the formation of two geometrical isomers for each complex. Interestingly, all complexes displayed three IR peaks for carbonyls ranging between 1857 and 2053 cm⁻¹. Similarly, a closer look at the ¹³C{¹H}-NMR spectra of complexes indicates the three carbonyl signals. Moreover, the ¹H and ¹³C{¹H}-NMR spectra of all complexes display two sets of peaks. All these observations support the formation of two geometrical isomeric species in each complex **Mn-1**, **Mn-2** and **Mn-3**. Considering the presence of three signals for carbonyls in each complex, we assume that one isomer of the Mn-complex would have two carbonyls that are *trans* to -Br and -N_{py} ligands accounting for two peaks (as indicated in the X-ray



Scheme 2 Synthesis of (R²PN³N^{Py}₂) manganese pincer complexes.





Fig. 1 ORTEP of compound **Mn-2** showing the atom-numbering scheme. Displacement ellipsoids are drawn at the 50% probability level. Selected bond length (Å): Br1–Mn1, 2.5916(7); Mn1–C9, 1.773(4); Mn1–C10, 1.797(4); Mn1–N3, 2.011(3); Mn1–N1, 2.012(3); Mn1–P1, 2.2462(12). Selected bond angles (°): N3–Mn1–P1, 160.49(11); C10–Mn1–N1, 175.88(16); C9–Mn1–Br1, 175.54(14); C9–Mn1–C10, 87.40(19); C9–Mn1–N1, 96.23(16); N1–Mn1–Br1, 84.57(9).

structure), whereas the other isomer would have two carbonyls *trans* to each other and display a single carbonyl peak (Scheme 2). Even though the assumed isomers are highly convincing, the probability of the mixture of a neutral (with –Br coordination) and a cationic (with Br as an anion) manganese species cannot be completely ruled out.^{11a,13b,16,17a} All the complexes are further characterized by ESI-MS that show two prominent isotopic

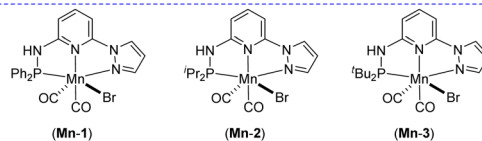
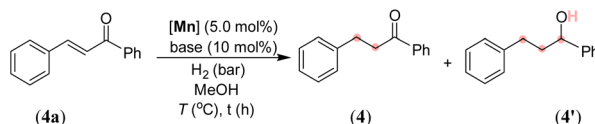
masses for ⁷⁹Br and ⁸¹Br containing complexes. The molecular structure of **Mn-2** was confirmed by a single crystal X-ray study (Fig. 1). As expected, the coordination geometry around the manganese is distorted octahedral with –Br and one –CO unit *trans* to each other, making the C9–Mn1–Br angle almost linear (175.54(15)°). The Mn1–C10 bond length (1.797(4) Å) is slightly longer than the Mn1–C9 bond length (1.773(4) Å), which might be due to the greater *trans* influence of –N_{py} than the –Br. Although each synthesized manganese complex contains two isomeric species, the generated active catalyst in the presence of a base is expected to be a single isomer (proved and discussed *vide infra*).

Optimization for catalytic hydrogenation

After synthesizing the sterically and electronically distinct mixed-donor (PN³N) manganese complexes, we have investigated their catalytic behavior for the chemoselective hydrogenation of α,β -unsaturated ketones using molecular hydrogen. We first screened the activity of (PN³N)Mn(I) complexes **Mn-1**, **Mn-2**, and **Mn-3** for C=C bond hydrogenation in (*E*)-3-phenyl-1-(phenyl)prop-2-en-1-one (**4a**) using a catalytic amount of KO^tBu and 30 bar hydrogen pressure in methanol at 50 °C (see, Tables 1 and S1 in the ESI[†]). The use of **Mn-1** as a catalyst led to 75% conversion of **4a**, wherein chemoselective C=C hydrogenated product **4** was obtained in 65% yield, and completely

Table 1 Optimization of reaction conditions^a

Entry	[Mn]	Base	<i>T</i> (°C)/ <i>t</i> (h)	Conv. ^b (%)	4 ^b (%)	4' ^b (%)
1	Mn-1	KO ^t Bu	50/20	75	65	10
2 ^c	Mn-2	KO ^t Bu	50/20	100	—	80
3	Mn-3	KO ^t Bu	50/20	100	63 (60)	37
4	Mn-3	KO ^t Bu	27/20	100	81 (79)	19
5	Mn-3	KO ^t Bu	27/20	100	91 (88)	9
6	Mn-3	NaO ^t Bu	27/20	40	39	Trace
7	Mn-3	LiO ^t Bu	27/20	74	73	Trace
8	Mn-3	K ₂ CO ₃	27/20	100	74	26
9	Mn-3	KOAc	27/20	20	19	Trace
10	Mn-3	K ₃ PO ₄	27/20	100	88	12
11	Mn-3	K ₃ PO ₄	27/1	100	98 (96)	2
12	Mn(CO) ₅ Br/L3	K ₃ PO ₄	27/1	39	39	—
13	MnBr ₂ /L3	K ₃ PO ₄	27/1	—	—	—
14	MnCl ₂ /L3	K ₃ PO ₄	27/1	—	—	—



^a Reaction conditions: **4a** (0.042 g, 0.20 mmol), base (0.02 mmol), [Mn] catalyst (0.01 mmol, 5 mol%), solvent (1.0 mL). Entries 1–4: 30 bar H₂; entries 5–10: 10 bar H₂; entries 11–14: 5 bar H₂. ^b GC conversion, isolated yields are given in parentheses. ^c 20% allylic alcohol was observed. All the catalysts **Mn-1**, **Mn-2** and **Mn-3** contain a mixture of two geometrical isomers.



hydrogenated compound **4'** in 10% yield (entry 1). The electronically rich complex **Mn-2** gave complete conversion of **4a**; however, the product **4'** was obtained in 80% yield, and the remaining was allylic alcohol with only C=O hydrogenation (entry 2). Interestingly, the bulky ^tBu-substituted complex **Mn-3** gave a complete conversion of **4a** with more chemoselectivity for **4** (entry 3). The formation of allylic alcohol in the presence of catalyst **Mn-2** suggests the probability of a sequential C=O hydrogenation-allylic alcohol isomerization leading to the uncontrolled hydrogenated compound **4'**. The low steric effect in complex **Mn-2** compared to **Mn-3** might play a crucial role in chemoselective hydrogenation (1,2-hydrogenation of C=O versus 1,4-hydrogenation of C=C). Notably, the reaction at lower hydrogen pressure and room temperature (27 °C) significantly improved chemoselective C=C bond hydrogenation without altering the overall conversion (entries 4 and 5). The use of other bases, such as NaO^tBu, LiO^tBu, and KOAc, led to low conversion, whereas the presence of mild bases K₂CO₃ or K₃PO₄ provided complete conversion with good chemoselectivity for **4** using 10 bar H₂ and at room temperature (entries 6–10). The activity of a manganese catalyst using a catalytic amount of mild base K₃PO₄ is notable, as most of the Mn catalysis generally employs a strong base like KO^tBu. The chemoselective hydrogenation of **4a** also proceeded smoothly using 5 bar hydrogen pressure at room temperature (27 °C) and provided **4** in 96% isolated yield just in an hour (entry 11). Notably, the manganese catalysts **Mn-1** and **Mn-2** were less effective for hydrogenation under the optimized conditions (5 bar H₂/27 °C/1 h), and provided <19% of product **4** (see the ESI†). Therefore, all chemoselective hydrogenations were conducted employing the **Mn-3** catalyst and 5 bar H₂ pressure at room temperature with the best-optimized reaction time. An *in situ* generated Mn(CO)₅Br/**L3** catalyst system is less effective, affording the hydrogenated product in 39% yield, highlighting the importance of a well-defined manganese catalyst (entry 12). However, a Mn(II) precursor with the **L3** ligand (MnCl₂/**L3** or MnBr₂/**L3**) did not provide hydrogenation (entries 13 and 14). Similarly, the Mn(CO)₅Br precursor and bidentate N-donor or P-donor ligand systems were ineffective. Hydrogenation did not proceed in the absence of a catalyst, a base or H₂, which suggests the importance of these components for the reaction.

Substrate scope of hydrogenation

After successfully optimizing the reaction parameters for chemoselective C=C bond hydrogenation in chalcone, we have explored the reaction scope using catalyst **Mn-3**, catalytic K₃PO₄ and 5 bar H₂ at room temperature (Scheme 3). Depending upon the substrates, the hydrogenations were performed for different time intervals, and the best yields were reported. First, we checked the hydrogenation of α,β -unsaturated ketones with different substitutions on the benzoyl ring. Thus, the chalcones containing electron-donating alkyl and alkoxy substitutions at the *para* position of benzoyl reacted smoothly to give a good to an excellent yield of saturated ketones **5–7**. The halogen substitutions, –Cl, –Br, –I, and –CF₃, were well tolerated at the *para* position of the benzoyl ring affording the desired saturated

ketones (**8–11**) in good yields. The tolerance of such functionalities is noteworthy as they can be employed for late-stage diversification. In addition to the *para*-substituted chalcones, the electron-rich and electron-deficient *ortho*-substituted compounds smoothly participated in hydrogenation (**12** and **13**). Chalcone having a phenolic –OH at the *meta* position of benzoyl, reacted slowly and afforded the product **14** in 33% yield. Interestingly, unsaturated ketones with sensitive and reducible functionalities, such as terminal alkene, alkyne, and epoxide, reacted chemoselectively to give compounds **15–17**. The unsaturated ketones with the naphthyl moiety also reacted with good yields (**18** and **19**). A higher-scale hydrogenation of compound **4a** (0.5 g, 2.4 mmol) provided the product **4** in 87% isolated yield (Scheme 3, in parenthesis), highlighting the potential practical application.

After this, we moved to check the effect and tolerability of different substitutions on the alkenyl-arenes towards chemoselective hydrogenation. Substrates with electron-rich substituents such as phenyl, methoxy and benzyloxy reacted efficiently, producing excellent yields of products **20–22**. The survival of benzyl protection of phenolic –OH is notable, as such substrates are prone to hydrogenolysis under hydrogenation conditions. Similarly, the –Cl and –CF₃ groups remained unaffected and delivered the saturated halo-ketones **23** and **24** in 80% and 96% yields, respectively. An amine functionality that could poison catalysis by binding to the metal is also sustained under optimized conditions (**25**). To our surprise, the highly desirous and hydrogenation-sensitive functionalities, –CN and –NO₂ groups, could be tolerated to afford the products **26** and **28** in around 88% yields. A range of α,β -unsaturated ketones derived from heteroarenes, such as furanyl, thiophenyl, indolyl, pyrrolyl and pyridinyl, were successfully hydrogenated to afford the saturated heteroaryl ketones (**30–35**). The chemoselective hydrogenation of these heteroaryl-containing compounds is remarkable, as the heteroaryl rings often interfere with the reaction due to their coordination ability to metal. The hydrogenation of ketones having unprotected NH indolyl and pyrrolyl opens up a new avenue as they can further be diversified. An unsaturated ketone containing a ferrocene backbone provided selective hydrogenation to **36** in 72% yield. Interestingly, hydrogenation of a ketone containing extended conjugation provided selectively semi-hydrogenated product **37** in 78% yield. Similarly, in the substrate where the carbonyl group is in conjugation with two alkenes, one C=C bond was selectively hydrogenated and provided a good yield of product **38**. This hydrogenation protocol is also suitable for α,β -unsaturated ketones having a trisubstituted alkene to provide saturated ketones, albeit in moderate yields (**39** and **40**). A β -alkyl- α,β -unsaturated ketone, (*E*)-1-phenyloct-2-en-1-one could be hydrogenated to give compound **41** in 75% yield. Interestingly, in all these cases, an excellent chemoselective C=C bond hydrogenation was observed in the presence of other H₂-sensitive functionalities. Such chemoselective hydrogenation employing a Mn-catalyst is extremely rare.^{11b,12c,13c} Unfortunately, the α,β -unsaturated ketones with free –OH at the *ortho* position, and carboxylate, ester and amide derivatives failed to participate in the reaction under the optimized conditions. However, the substrate (*E*)-4-phenylbut-





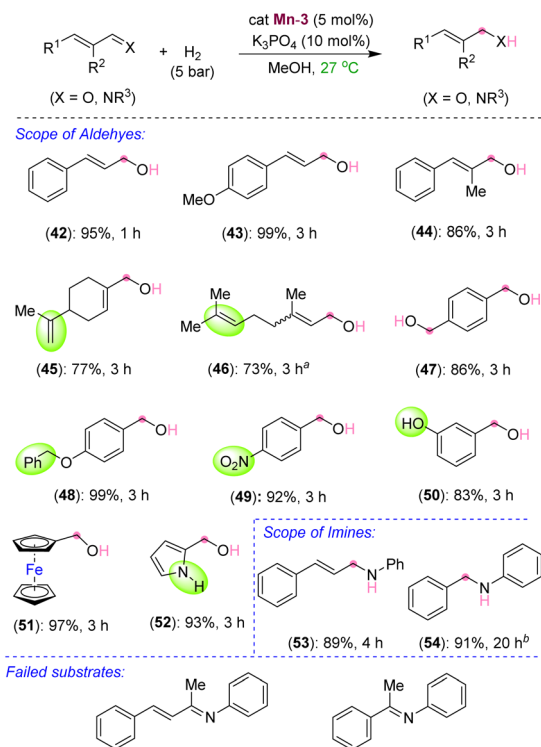
Scheme 3 Scope of Mn-catalyzed C=C bond hydrogenation of α,β -unsaturated ketones. Reaction conditions: substrate, α,β -unsaturated ketone (0.20 mmol), Mn-3 (0.005 g, 0.01 mmol, 5 mol%), K_3PO_4 (0.0043 g, 0.02 mmol), MeOH (1.0 mL), H_2 (5 bar). Yields are of isolated compounds. ^aReaction in 0.5 g scale. ^bReaction at 50 $^\circ\text{C}$. ^cMixture of MeOH : DCM (4 : 1) used. ^dReaction at 10 bar H_2 and 50 $^\circ\text{C}$.

3-en-2-one gave a mixture of highly unselective hydrogenated products.

After exploring the scope and limitations of selective C=C bond hydrogenation in unsaturated ketones, we were eager to know the reactivity of the synthesized manganese complex on the hydrogenation of α,β -unsaturated aldehydes and imines (Scheme 4). Surprisingly, under the standard reaction conditions, selective C=O bond hydrogenation of cinnamaldehyde derivatives was observed, leading to the 3-phenylprop-2-en-1-ols (42–44) in excellent yields. Aliphatic and acyclic conjugated

aldehydes also participated in the selective hydrogenation to unsaturated alcohols without harming the alkenyl groups, thus leading to the products 45 and 46 in 77% and 73% yields, respectively. The aromatic aldehydes containing benzyloxy, nitro, –OH, and pyrrolyl groups were also smoothly hydrogenated to the corresponding alcohols at room temperature (48–52). The tolerance of free –OH and –NH groups is highly impressive. Similarly, an α,β -unsaturated imine was chemoselectively hydrogenated to unsaturated amine (53) in good yield. Even a simple unconjugated *N*-aryl imine could be





Scheme 4 Scope of Mn-catalyzed hydrogenation of aldehydes and imines. ^aReaction conditions: substrate (0.20 mmol), **Mn-3** (0.005 g, 0.01 mmol, 5 mol%), K₃PO₄ (0.0043 g, 0.02 mmol), H₂ (5 bar), MeOH (1.0 mL). Yields are of isolated compounds. ^bObtained as a mixture of *E* and *Z* isomers as the starting compound was also a mixture of both. ^bReaction performed at 50 °C.

hydrogenated to amine in high yield (**54**). However, the attempted hydrogenations of ketone-derived imine analogues, such as (*2E,3E*)-*N,4*-diphenylbut-3-en-2-imine and (*E*)-*N,1*-diphenylethan-1-imine, failed under the optimized conditions and the unreacted starting compounds were quantitatively recovered (Scheme 4). We assume that the steric hindrance around the keto-derived imine inhibited its approach towards the manganese center, leading to an unsuccessful reaction. The chemoselective hydrogenations of the C=C bond over the ketone carbonyl and that of the aldehyde's C=O and imine's C=N over the C=C by using the newly developed catalyst are notable. Particularly, mild reaction conditions and the use of the catalytic K₃PO₄ base are significant. This catalyst can further be applied to novel catalytic approaches considering its advantage over other similar catalysts. Though, an excellent chemoselectivity was observed in the hydrogenation of α,β -unsaturated ketones, a trace formation of both C=C and C=O reductions was unavoidable in some cases.

Mechanistic aspects

We have performed a few controlled experiments to understand the operating mode of the manganese catalyst. First, the *N*-methyl substituted ligand (**L3-Me**) and corresponding manganese complex, (^tBuPN(Me)N^{PyZ})Mn(CO)₃Br (**Mn-3^{Me}**) were



Scheme 5 Synthesis of **Mn-3^{Me}** and controlled mechanistic experiments.

synthesized and fully characterized by various analytical techniques (Scheme 5a). An attempted hydrogenation of **4a** employing complex **Mn-3^{Me}** as the catalyst under the standard hydrogenation conditions did not provide the hydrogenated product (Scheme 5b), and the starting compound (**4a**) was quantitatively recovered. This finding supports the crucial role of the N–H proton in the complex (^tBuPN³(H)N^{PyZ})Mn(CO)₂Br (**Mn-3**) during hydrogenation. Furthermore, the treatment of **Mn-3** with stoichiometric KO^tBu produced dearomatized active intermediate **A** (Fig. 2). The ³¹P{¹H} NMR spectrum of **A** showed a single peak (against two isomeric peaks for **Mn-3**), and two CO signals were observed in IR as well as ¹³C{¹H} NMR spectra of **A** (against three peaks for CO in **Mn-3**). Interestingly, the employment of species **A** as a catalyst in hydrogenation without the use of an additional base provided a quantitative yield of **4**. All these results suggest that the species **A** acts as an active catalyst and the catalytic reaction proceeds through the metal–ligand cooperation (dearomatization/aromatization) pathway.

A hydrogenation reaction was performed using CD₃OD as a solvent to thoroughly understand the hydrogenation process (Scheme 5c). The isolated hydrogenated product **4**-[D] shows 92% deuterium incorporation at the alpha-methylene position (see ¹H, ¹³C and deuterium NMR spectra in the ESI†). Moreover, the hydrogenation reaction did not occur in the presence of aprotic solvent (THF, dioxane or CH₂Cl₂). These observations indicate the necessity of a protic solvent as a proton source and





Fig. 2 Synthesis of active intermediate A and characterization spectra.

tentatively support a Mn-enolate intermediate. All these findings are consistent with the low energy barrier observed for the protonation step (discussed *vide infra*). An attempted hydrogenation of allylic alcohol under the standard reaction conditions failed to give a hydrogenated product (Scheme 5d). This finding highlights that the hydrogenation of (*E*)-chalcone (**4a**) does not proceed *via* 1,2-hydrogen addition, instead a 1,4-addition of hydrogen occurs. The observed chemoselectivity and controlled studies allowed us to propose the following: (i) the **Mn-3** catalyst prefers 1,2-hydrogen addition to C=O or C=N when steric hindrance on carbonyl's/imine's carbon is low (aldehyde's C=O and imine's C=N preferred over the C=C), whereas (ii) the **Mn-3** catalyst allowed 1,4-hydrogen addition when carbonyl's carbon is doubly substituted (*i.e.* in α,β -unsaturated ketones) due to more steric constraint. Mn-H might fail to approach the carbonyl's carbon in α,β -unsaturated ketones due to steric hindrance; instead it can access the β -carbon *via* 1,4-hydrogen addition. Notably, the **Mn-2** catalyst, which is less bulky than the **Mn-3** catalyst, allowed 1,2-hydrogen addition even in α,β -unsaturated ketone to form allylic alcohol. These findings are noteworthy in the consideration of catalyst developments for chemoselective functionalization.

DFT based calculations

We have investigated the reaction mechanism of **Mn-3** catalyzed hydrogenation of α,β -unsaturated carbonyl compound **4a** using density functional theory (DFT) calculations (Fig. 3). Initially, the generation of the active catalyst **A** would occur when the pre-catalyst **Mn-3** reacts with K_3PO_4 (Fig. 3(I)). In this step, the Mn-Br and N-H bonds break, forming the catalyst **A**, K_2HPO_4 and KBr. This step is thermodynamically favorable ($\Delta G = -19.9 \text{ kcal mol}^{-1}$). Next, the H_2 molecule adds to catalyst **A**, forming the intermediate **B** *via* a barrier of $14.7 \text{ kcal mol}^{-1}$ (**TS-1**). Then, the reaction proceeds through **TS-2** with a barrier of $21.7 \text{ kcal mol}^{-1}$, in which the H-H bond breaks, and the Mn-H and N-H bonds form, generating the intermediate **C**. The overall barrier for the H_2 activation ($31.3 \text{ kcal mol}^{-1}$) seems reasonable, considering that a minimum of 5 bar H_2 pressure is essential for the reaction. In the next step, the reaction crosses the barrier of $9.1 \text{ kcal mol}^{-1}$ (**TS-3**), wherein **4a** reacts with **C** to form the intermediate **D** by hydride (H^-) migration from Mn-H to **4a**. In the next step, the intermediate **D** rearranges and forms a new intermediate **E**. This step is found to be thermodynamically favorable ($\Delta G = -5.2 \text{ kcal mol}^{-1}$).

Starting with the intermediate **E**, two approaches are considered for protonation (Fig. 3(II)). In the first possibility, the methanol protonates the substrate step-wise, as shown in Fig. 3(II). Thus, MeOH can provide a proton to the substrate and coordinates with Mn concurrently. In this process, the Mn-O bond breaks and a different Mn-O bond forms *via* the transition state **TS-4** with a barrier of $10.7 \text{ kcal mol}^{-1}$, leading to the formation of the intermediate **F**. The reaction crosses a barrier of $1.1 \text{ kcal mol}^{-1}$ (**TS-5**) in the following step, leading to product **4** and intermediate **G**. Then, the reaction could proceed in two different ways: with the assistance of solvent (MeOH) **TS-6** and without the assistance of solvent **TS-6'**, which has barriers of $6.8 \text{ kcal mol}^{-1}$ and $14.6 \text{ kcal mol}^{-1}$, respectively. The energy values indicate that the reaction will proceed through the transition state **TS-6** with the assistance of a solvent (MeOH), leading to the formation of intermediate **H**. In the next step, intermediate **H** is converted into **A** after releasing methanol. This step is thermodynamically favorable ($\Delta G = -4.4 \text{ kcal mol}^{-1}$). The overall low barrier for the protonation process tentatively supports the experimental observation, wherein a reversible protonation was assumed.

In the second possibility of protonation, the solvent MeOH directly shuttles the protons between Mn-O and N-H through a transition state **TS-7** with a barrier of $11.0 \text{ kcal mol}^{-1}$, leading to the formation of intermediate **I** (Fig. 3(II)). In the next step, intermediate **I** is converted into the active species **A** and product **4**. This step is thermodynamically favorable ($\Delta G = -18.5 \text{ kcal mol}^{-1}$). A perusal of the two pathways based on turnover frequency (TOF) analysis indicates that the TOF would be the same for both approaches (Fig. 3(II)), because the main intermediate (TDI) (**A**) along the pathways and the main transition state (TDTS) (**TS-2**) are present in the early part of the cycles, which are common to both the proposed protonation pathways (for more information on the TOF analysis, see the ESI†). The calculated energy barrier values indicated a maximum barrier for H_2 activation, which would be feasible at room temperature considering the reaction's 5.0 bar H_2





Fig. 3 Free energy profile for $(tBu_2PNNPy)_2Mn(I)$ -catalyzed hydrogenation: (I) Mn-3 to intermediate E, (II) intermediate E to regeneration of active catalyst A. The free energy values are given in kcal mol⁻¹.

pressure requirement. Therefore, H_2 activation could be proposed as a probable turnover-limiting step. Notably, the protonation of the final compound by MeOH is very facile, which corroborates the experimental findings.

Catalytic cycle

Based on the experimental findings, DFT calculations and literature precedents,^{12a,15c,21b} we proposed a tentative catalytic cycle for the Mn-catalyzed chemoselective hydrogenation of α,β -unsaturated ketones (Fig. 4). Initially, the complex **Mn-3** would transform into the active catalyst **A** by dearomatization in the presence of K_3PO_4 . We have identified the species **A** by NMR and IR analyses. The similar conversion of a metal complex into dearomatized species is well documented.^{12a,21b,24} Moreover, the

species **A** as an active catalyst was verified. The H_2 molecule will coordinate to Mn(I) species, followed by metal–ligand (M–L) cooperative activation of H_2 leading to species **C** through transition state **TS-2**. Next, the reaction of substrate **4a** with **C** leads to 1,4-hydride migration resulting in intermediate **D** (or **E**). The protonation of the semi-hydrogenated species in intermediate **D** (or **E**) by methanol provides the hydrogenated product **4**. Finally, the resulting intermediate **G** would lead to the regeneration of active catalyst **A**. The DFT energy calculations supported all these elementary catalytic steps. H_2 activation by the Mn(I) species has a high barrier and is a pivotal step in the hydrogenation process. Therefore, H_2 activation by Mn(I)–ligand cooperation can be assumed to be the turnover-limiting step.



- 5 (a) G. A. Filonenko, R. van Putten, E. J. M. Hensen and E. A. Pidko, *Chem. Soc. Rev.*, 2018, **47**, 1459–1483; (b) T. Zell and R. Langer, *ChemCatChem*, 2018, **10**, 1930–1940; (c) L. Alig, M. Fritz and S. Schneider, *Chem. Rev.*, 2019, **119**, 2681–2751; (d) T. Irrgang and R. Kempe, *Chem. Rev.*, 2019, **119**, 2524–2549.
- 6 (a) I. Bauer and H.-J. Knölker, *Chem. Rev.*, 2015, **115**, 3170–3387; (b) T. Zell and D. Milstein, *Acc. Chem. Res.*, 2015, **48**, 1979–1994; (c) S. Chakraborty, P. Bhattacharya, H. Dai and H. Guan, *Acc. Chem. Res.*, 2015, **48**, 1995–2003; (d) A. Fürstner, *ACS Cent. Sci.*, 2016, **2**, 778–789.
- 7 (a) A. Mukherjee and D. Milstein, *ACS Catal.*, 2018, **8**, 11435–11469; (b) W. Liu, B. Sahoo, K. Junge and M. Beller, *Acc. Chem. Res.*, 2018, **51**, 1858–1869; (c) W. Ai, R. Zhong, X. Liu and Q. Liu, *Chem. Rev.*, 2019, **119**, 2876–2953.
- 8 (a) R. M. Bullock, *Science*, 2013, **342**, 1054–1055; (b) W. Zuo, A. J. Lough, Y. F. Li and R. H. Morris, *Science*, 2013, **342**, 1080–1083; (c) M. R. Friedfeld, M. Shevlin, J. M. Hoyt, S. W. Krska, M. T. Tudge and P. J. Chirik, *Science*, 2013, **342**, 1076–1080; (d) M. R. Friedfeld, H. Zhong, R. T. Ruck, M. Shevlin and P. J. Chirik, *Science*, 2018, **360**, 888–893.
- 9 S. Elangovan, C. Topf, S. Fischer, H. Jiao, A. Spannenberg, W. Baumann, R. Ludwig, K. Junge and M. Beller, *J. Am. Chem. Soc.*, 2016, **138**, 8809–8814.
- 10 F. Kallmeier, T. Irrgang, T. Dietel and R. Kempe, *Angew. Chem., Int. Ed.*, 2016, **55**, 11806–11809.
- 11 (a) A. Bruneau-Voisine, D. Wang, T. Roisnel, C. Darcel and J.-B. Sortais, *Catal. Commun.*, 2017, **92**, 1–4; (b) D. Wei, A. Bruneau-Voisine, T. o. Chauvin, V. Dorcet, T. Roisnel, D. A. Valyaev, N. I. Lugan and J.-B. Sortais, *Adv. Synth. Catal.*, 2018, **360**, 676–681; (c) R. Buhaibeh, O. A. Filippov, A. Bruneau-Voisine, J. Willot, C. Duhayon, D. A. Valyaev, N. Lugan, Y. Canac and J.-B. Sortais, *Angew. Chem., Int. Ed.*, 2019, **58**, 6727–6731; (d) R. Buhaibeh, C. Duhayon, D. A. Valyaev, J.-B. Sortais and Y. Canac, *Organometallics*, 2021, **40**, 231–241.
- 12 (a) M. Glatz, B. Stöger, D. Himmelbauer, L. F. Veiros and K. Kirchner, *ACS Catal.*, 2018, **8**, 4009–4016; (b) S. Weber, B. Stöger and K. Kirchner, *Org. Lett.*, 2018, **20**, 7212–7215; (c) S. Weber, J. Brünig, L. F. Veiros and K. Kirchner, *Organometallics*, 2021, **40**, 1388–1394.
- 13 (a) H.-J. Pan and X. Hu, *Angew. Chem., Int. Ed.*, 2020, **59**, 4942–4946; (b) W. Yang, I. Y. Chernyshov, R. K. A. van Schendel, M. Weber, C. Müller, G. A. Filonenko and E. A. Pidko, *Nat. Commun.*, 2021, **12**, 12; (c) T. Vielhaber and C. Topf, *Appl. Catal. A: Gen.*, 2021, **623**, 118280.
- 14 For reviews, see: (a) B. Maji and M. K. Barman, *Synthesis*, 2017, **49**, 3377–3393; (b) M. Garbe, K. Junge and M. Beller, *Eur. J. Org. Chem.*, 2017, **2017**, 4344–4362; (c) F. Kallmeier and R. Kempe, *Angew. Chem., Int. Ed.*, 2018, **57**, 46–60; (d) N. Gorgas and K. Kirchner, *Acc. Chem. Res.*, 2018, **51**, 1558–1569.
- 15 (a) D. Wei, A. Bruneau-Voisine, D. A. Valyaev, N. Lugan and J.-B. Sortais, *Chem. Commun.*, 2018, **54**, 4302–4305; (b) Y. Wang, L. Zhu, Z. Shao, G. Li, Y. Lan and Q. Liu, *J. Am. Chem. Soc.*, 2019, **141**, 17337–17349; (c) F. Freitag, T. Irrgang and R. Kempe, *J. Am. Chem. Soc.*, 2019, **141**, 11677–11685; (d) Z. Wang, L. Chen, G. Mao and C. Wang, *Chin. Chem. Lett.*, 2020, **31**, 1890–1894; (e) Y. Wang, S. Liu, H. Yang, H. Li, Y. Lan and Q. Liu, *Nat. Chem.*, 2022, **14**, 1233–1241.
- 16 M. B. Widegren, G. J. Harkness, A. M. Z. Slawin, D. B. Cordes and M. L. Clarke, *Angew. Chem., Int. Ed.*, 2017, **56**, 5825–5828.
- 17 (a) M. Garbe, K. Junge, S. Walker, Z. Wei, H. Jiao, A. Spannenberg, S. Bachmann, M. Scalone and M. Beller, *Angew. Chem., Int. Ed.*, 2017, **56**, 11237–11241; (b) M. Garbe, Z. Wei, B. Tannert, A. Spannenberg, H. Jiao, S. Bachmann, M. Scalone, K. Junge and M. Beller, *Adv. Synth. Catal.*, 2019, **361**, 1913–1920.
- 18 (a) L. Zhang, Y. Tang, Z. Han and K. Ding, *Angew. Chem., Int. Ed.*, 2019, **58**, 4973–4977; (b) L. Zhang, Z. Wang, Z. Han and K. Ding, *Angew. Chem., Int. Ed.*, 2020, **59**, 15565–15569.
- 19 (a) F. Ling, H. Hou, J. Chen, S. Nian, X. Yi, Z. Wang, D. Song and W. Zhong, *Org. Lett.*, 2019, **21**, 3937–3941; (b) L. Zeng, H. Yang, M. Zhao, J. Wen, J. H. R. Tucker and X. Zhang, *ACS Catal.*, 2020, **10**, 13794–13799; (c) F. Ling, J. Chen, S. Nian, H. Hou, X. Yi, F. Wu, M. Xu and W. Zhong, *Synlett*, 2020, **31**, 285–289; (d) C. S. G. Seo, B. T. H. Tsui, M. V. Gradiski, S. A. M. Smith and R. H. Morris, *Catal. Sci. Technol.*, 2021, **11**, 3153–3163.
- 20 (a) C. Liu, M. Wang, S. Liu, Y. Wang, Y. Peng, Y. Lan and Q. Liu, *Angew. Chem., Int. Ed.*, 2021, **60**, 5108–5113; (b) C. Liu, M. Wang, Y. Xu, Y. Li and Q. Liu, *Angew. Chem., Int. Ed.*, 2022, **61**, DOI: [10.1002/anie.202202814](https://doi.org/10.1002/anie.202202814).
- 21 (a) S. Weber, B. Stöger, L. F. Veiros and K. Kirchner, *ACS Catal.*, 2019, **9**, 9715–9720; (b) S. M. W. Rahaman, D. K. Pandey, O. Rivada-Wheelaghan, A. Dubey, R. R. Fayzullin and J. R. Khusnutdinova, *ChemCatChem*, 2020, **12**, 5912–5918.
- 22 For selected chemoselective hydrogenation using **4d** metals, see: (a) Q. Hu, Y. Hu, Y. Liu, Z. Zhang, Y. Liu and W. Zhang, *Chem.–Eur. J.*, 2017, **23**, 1040–1043; (b) W. Chang, X. Gong, S. Wang, L.-P. Xiao and G. Song, *Org. Biomol. Chem.*, 2017, **15**, 3466–3471; (c) M. Soto, R. G. Soengas and H. Rodríguez-Solla, *Adv. Synth. Catal.*, 2020, **362**, 5422–5431; (d) Y. Gu, J. R. Norton, F. Salahi, V. G. Lisnyak, Z. Zhou and S. A. Snyder, *J. Am. Chem. Soc.*, 2021, **143**, 9657–9663.
- 23 (a) D. Gong, W. Liu, T. Chen, Z.-R. Chen and K.-W. Huang, *J. Mol. Catal. A Chem.*, 2014, **395**, 100–107; (b) D. Gong, X. Zhang and K.-W. Huang, *Dalton Trans.*, 2016, **45**, 19399–19407; (c) H. Chen, W. Pan, K.-W. Huang, X. Zhang and D. Gong, *Polym. Chem.*, 2017, **8**, 1805–1814.
- 24 (a) T. P. Gonçalves and K.-W. Huang, *J. Am. Chem. Soc.*, 2017, **139**, 13442–13449; (b) T. Shimbayashi and K.-i. Fujita, *Catalysts*, 2020, **10**, 635.

